Large interannual variations in nonmethane volatile organic compound emissions based on measurements of carbon monoxide

Keyhong Park,[1,2] Louisa K. Emmons,[3] Zhihui Wang,[1] and John E. Mak[1]

Received 23 September 2012; revised 16 November 2012; accepted 24 November 2012; published 16 January 2013.

[1] We present source estimates of atmospheric carbon monoxide from nonmethane volatile organic compound (NMVOC) oxidation during a period of 8 years (1997–2004) using a Bayesian inversion analysis. The optimized global NMVOC-derived CO source strength indicates a change of a factor of 2 between the 1997–1998 strong El Niño and subsequent La Niña conditions. For comparison, the average 8 year interannual variability (IAV) is 18%. The variation of NMVOC-derived CO is closely correlated with the Oceanic Niño Index (ONI) and surface temperature. A time-lagged correlation analysis between ONI and NMVOC-derived CO inventory indicated El Niño/Southern Oscillation leads the Northern Hemisphere (NH) NMVOC-derived CO production by about 3 months earlier than the Southern Hemisphere's (SH). The SH NMVOC-derived CO was positively correlated with the lagged-ONI ($r = 0.57$), while the temperature change barely influenced SH NMVOC-derived CO ($r = 0.01$). In the NH, temperature was more robustly correlated with NMVOC-derived CO ($r = 0.58$) than the lagged-ONI ($r = 0.35$). In particular, the extra-tropical temperature showed a strong correlation ($r = 0.90$) with the NH NMVOC-derived CO and suggested its primary role in controlling the interannual variability of the NH NMVOC-derived CO.
Citation: Park, K., L. K. Emmons, Z. Wang, and J. E. Mak (2013), Large interannual variations in nonmethane volatile organic compound emissions based on measurements of carbon monoxide, *Geophys. Res. Lett.*, *40*, 221–226, doi:10.1029/2012GL052303.

1. Introduction

[2] Temporal and spatial variations in atmospheric CO concentration are often correlated with its sources. It is known that methane oxidation, nonmethane volatile organic compound (NMVOC) oxidation, biomass burning, and fossil fuel and biofuel combustion are the major sources of CO [*Bergamaschi et al*., 2000; *Pétron et al*., 2002; *Duncan et al*., 2007]. Recent studies have improved CO inventories for anthropogenic and biomass burning CO emissions [*Olivier and Berdowski*, 2001; *Pétron et al*., 2004; *Arellano et al*., 2006; *van der Werf et al*., 2006; *Ohara, et al*., 2007]. Production of CO from methane oxidation can be calculated quite accurately due to the long lifetime of atmospheric CH_4 (~10 years) and the concomitant homogeneous distribution [*Lawrence et al*., 2001; *Horowitz et al*., 2003; *Emmons et al*., 2010]. Unlike the other major sources, CO from NMVOC oxidation has not been well constrained and there exists a large range in its estimates (see Table S1 in the Supporting Information) [*Bergamaschi et al*., 2000; *Kasibhatla et al*., 2002; *Arellano et al*., 2004; *Müller and Stavrakou*, 2005; *Arellano et al*., 2006].

[3] The majority of NMVOCs are emitted from vegetation; a small amount, on the order of 10%, is emitted from human activities [*Duncan et al*., 2007; *Goldstein and Galbally*, 2007]. Isoprene is by far the most abundant NMVOC emitted from the biosphere. Biogenic NMVOC emissions are sensitive to climatic conditions such as temperature, sunlight, soil water content, and leaf area index (LAI). While NMVOCs impact regional atmospheric chemistry and climate [*Shindell et al*., 2007; *Shindell et al*., 2008], their short lifetimes (minutes to days), low concentrations, and myriad individual species make quantification on a large scale challenging. NMVOCs react with atmospheric oxidants such as hydroxyl radicals and ozone, and are largely oxidized to carbon monoxide, whose lifetime is relatively long (2–3 months, global, annual average). Thus, a combined model-observation study of atmospheric CO may shed light on the temporally varying hemispheric and global emission of NMVOCs.

[4] Most of the NMVOC-derived CO is produced from oxidation of isoprene, monoterpenes, and methanol. It is currently thought that isoprene is responsible for 40–65% of total biogenic NMVOC emissions, with monoterpenes and methanol comprising most of the remainder [*Guenther et al*., 1995; *Guenther et al*., 2006; *Fowler et al*., 2009]. The globally averaged yield of CO from isoprene oxidation has been reported to be 0.2–0.34 [*Miyoshi et al*., 1994; *Bergamaschi et al*., 2000; *Granier et al*., 2000; *Duncan et al*., 2007; *Pfister et al*., 2008] and less than 0.2 in tropical regions, where the majority (70–80%) of isoprene is emitted [*Guenther et al*., 2006; *Fowler et al*., 2009]. The yield of CO from methanol oxidation, on the other hand, is estimated to be close to 1 [*Duncan et al*., 2007]. Therefore, a variation in the amount of NMVOC-derived CO may result from either a change in magnitude or variation in the type of NMVOC being emitted (or both).

[5] In this study, source strengths of CO are optimized for the 1997–2004 period using both observations and MOZART-4 (Model for Ozone and Related chemical Tracers) [*Emmons et al*., 2010] simulation results. We focus on the NMVOC oxidation source since it has not been well

All Supporting Information may be found in the online version of this article.

[1]Institute for Terrestrial and Planetary Atmospheres/School of Marine and Atmospheric Sciences, State University of New York at Stony Brook, Stony Brook, New York, USA.
[2]Division of Polar Climate Research, Korea Polar Research Institute, Incheon, South Korea.
[3]Atmospheric Chemistry Division, National Center for Atmospheric Research, Boulder, Colorado, USA.

Corresponding author: K. Park, Division of Polar Climate Research, Korea Polar Research Institute, Incheon, South Korea. (keyhongpark@kopri.re.kr)

0094-8276/13/2012GL052303

constrained and its interannual variability (IAV) has been previously investigated only by models. This time period covers the very strong 1997–1998 El Niño and the subsequent La Niña, which allows for an evaluation of the IAV of NMVOC-derived CO resulting from different climate conditions. To explain the multiyear change of NMVOC-derived CO, we examine the correlation of NMVOC-derived CO with ONI and temperature, which are two main proxies of climatic conditions and biogenic NMVOC emissions.

2. Data and Methods

[6] We use monthly averages of NOAA Global Monitoring Division (GMD) CO weekly flask samples [GLOBALVIEW-CO, 2009] for the observational data; 11 Northern Hemispheric (NH) and 4–9 Southern Hemispheric (SH) background CO stations are selected depending on the data availability (see Table S2 in the Supporting Information for information of sampling stations). Nonbackground CO data influenced by sampling artifacts or regional pollution are rejected by a rigorous analytic quality control and H_2 measurement (>800 ppbv). Also, data points lying outside of 3σ from a smooth curve fit are considered not representative of clean air and removed from the observational data set [*Novelli et al*., 1998].

[7] A tracer version of the global chemical transport model MOZART-4 is used for this study. This version contains chemical reactions and species only directly related to carbon monoxide. It has a simplified chemistry scheme and uses prescribed OH concentrations and CO chemical production rates, which are from a simulation using the full-chemistry version of MOZART-4. The OH fields and CO production rates are monthly averages that match the dates of the tracer simulation, i.e., they include interannual variation. The tracer version is computationally faster than the regular version of MOZART-4 and the results can be more efficiently analyzed. Each source of CO is tagged and was treated as an independent tracer with the same reaction rates and deposition velocities as CO.

[8] The model has a horizontal resolution of $2.8^\circ \times 2.8^\circ$ and 28 vertical levels from the surface to the top of the stratosphere (2 hPa). The meteorology is driven by the NCAR reanalysis of the National Centers for Environmental Prediction forecasts (NCEP/NCAR reanalysis) [*Kalnay et al*., 1996; *Kistler et al*., 2001]. The model simulation time period is from April 1996 through December 2004. The model reproduced the observations fairly well and the correlation between modeled and observed CO is 0.94, mean difference is 10.5 ppbv and chi-square is 0.65.

[9] The sources of CO are separated into seven categories: methane oxidation; NMVOC oxidation; biomass burning; fossil fuel combustion; biofuel use; and direct emission from plants and the ocean. The monthly emission inventory of anthropogenic sources (fossil fuel combustion and biofuel use) is from *Pétron et al*. [2004]. The Global Fire Emissions Database version 2 [*van der Werf et al*., 2006] inventory is used for the biomass burning source of CO. Carbon monoxide from methane oxidation is calculated on-line. Surface methane concentrations are set to the zonal average of the monthly mean NOAA GMD surface measurements. NMVOC-derived CO is calculated by subtracting modeled methane-derived CO from the total chemical CO production (hydrocarbon oxidation) taken from the full-chemistry MOZART-4 runs. The included chemical mechanism for NMVOC oxidation is described in *Emmons et al*. [2010]. The inventories of oceanic and biogenic sources are taken from the POET inventory [*Olivier et al*., 2003].

[10] To constrain the NMVOC oxidation source of CO, a Bayesian synthesis inversion is applied. This technique constrains the *a priori* sources by combining observed and modeled information, and has been used to constrain CO sources in previous studies [*Bergamaschi et al*., 2000; *Pétron et al*., 2002; *Arellano et al*., 2004; *Müller and Stavrakou*, 2005; *Arellano et al*., 2006]. A Bayesian inversion finds a matrix of optimized source strengths ($\hat{\mathbf{x}}$) from the following equation:

$$\hat{\mathbf{x}} = \mathbf{x_a} + \left(\mathbf{K^T S_e^{-1} K} + \mathbf{S_a^{-1}}\right)^{-1} \mathbf{K^T S_e^{-1}} (\mathbf{y - K x_a}) \quad (1)$$

where $\mathbf{x_a}$ denotes a matrix of *a priori* source strength estimates, $\mathbf{S_e}$ is the error covariance matrix of the model, $\mathbf{S_a}$ is the error covariance matrix of prior information, $\mathbf{y}$ is the observation, and $\mathbf{K}$ is the Jacobian matrix that links concentration and source strength calculated from the forward model.

[11] A detailed discussion about the evaluation and magnitude of the uncertainties in observations and *a priori* source strengths ($\mathbf{S_e}$ and $\mathbf{S_a}$) is presented in [*Park*, 2010]. Briefly, the observation error ($\mathbf{S_e}$), which is comprised of measurement error, representation error, and forward model error is assumed to be a diagonal and is estimated to be 15%. The past source strength estimates ranged within 15% to 100% (Table S1) for each source and the previous inversion studies assigned typically 50% for the uncertainty level of the *a priori* source strength ($\mathbf{S_a}$) [*Palmer et al*., 2003; *Arellano et al*., 2004; *Heald et al*., 2004; *Arellano et al*., 2006; *Duncan et al*., 2007]. In this study, $\mathbf{S_a}$ is assumed diagonal and estimated at 50% for each source but 10% is assigned for methane oxidation source and 20% is assigned for fossil fuel source because they are relatively well characterized.

[12] Since NMVOC-derived CO is tagged in the model simulation, interannual variations of this source can be quantitatively determined. During the model simulation period (1997–2004), inversion analyses were performed for every 6 months interval with 1 year of observations estimating one year's source inventory (ex. Jan. 1997 to Dec. 1997, Jul. 1997 to Jun. 1998,. . .Jan. 2004 to Dec. 2004). Each analysis was done on a hemispheric scale. Thus, observations of CO in each hemisphere are used to constrain the source strengths of that hemisphere only, since the lifetime of NMVOC is short and the interhemispheric mixing of CO is very limited [*Mak and Brenninkmeijer*, 1998; *Staudt et al*., 2001; *Williams et al*., 2002].

3. Results and Discussion

[13] The optimized global mean source strengths during the inversion analysis period (1997–2004) are presented in Table S1 and Figure S1. These values are consistent with previous CO source strength estimates, also shown in Table S1. To quantify the IAV of each CO source, IAV is defined as one standard deviation about the 1997–2004 mean, expressed in percent [*Palmer et al*., 2006]. The IAV of biomass burning (26.3%) and NMVOC oxidation (17.5%) sources were relatively large in comparison with methane oxidation (1.5%) and anthropogenic emission (6.0%). Especially, during the 1997 strong El Niño year and following

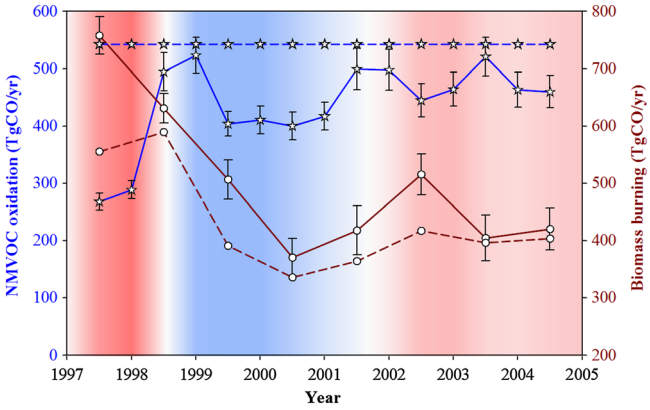

Figure 1. *A priori* (dashed lines) and *a posteriori* (solid lines) global CO source strengths from biomass burning (red) and NMVOC oxidation (blue). Shaded background shows ONI and the color intensity corresponds to the strength of El Niño (red) and La Niña (blue) condition. The error bars are *a posteriori* errors derived from the inversion analyses.

long La Niña conditions (1997–2000), NMVOC oxidation and biomass burning sources showed maximum fluctuation, which varied 95% and 65%, respectively. While the large IAV of biomass burning CO has been known [*van der Werf et al.*, 2006] and already considered in the *a priori* emissions of the model, the large IAV of NMVOC-derived CO was derived from the *a priori* inventory (Figure 1).

[14] High global isoprene emissions during El Niño events and low global isoprene emissions during La Niña events have been reported from several modeling studies [*Naik et al.*, 2004; *Lathière et al.*, 2006; *Müller et al.*, 2008]. Model simulations indicate a ~13% enhanced global isoprene emission during the 1997–1998 El Niño and large IAV (~20%) of the emission during 1995–2006 [*Müller et al.*, 2008]. *Müller et al.*, [2008] also reported there was approximately a 6 month delay between isoprene emission and changes in the ONI (Oceanic Niño Index; [*Smith et al.*, 2008]). Because other biogenic VOCs, including monoterpenes and methanol are also sensitive to changes in climate factors [*Guenther et al.*, 1995; *Wang et al.*, 1998; *Tie et al.*, 2003; *Guenther et al.*, 2006; *Lathière et al.*, 2006], we plot NMVOC-derived CO with ONI in Figure 2 to examine the influence of El Niño/Southern Oscillation (ENSO) to the global NMVOC-derived CO inventory. Our lag-correlation analysis between ONI and NMVOC-derived CO inventory (right panes in Figure 2) suggests ENSO leads NMVOC-derived CO production by about 11 months in the NH and 14 months in the SH. However, when the two periods (1/97 to 12/97 and 6/97 to 7/98) influenced by strong El Niño and severe drought [*Haddad et al.*, 2004] are removed, the best correlation appears earlier and is more robust (NH: 7 months lag, $r = 0.67$; SH: 13 months lag, $r = 0.66$). The temporal

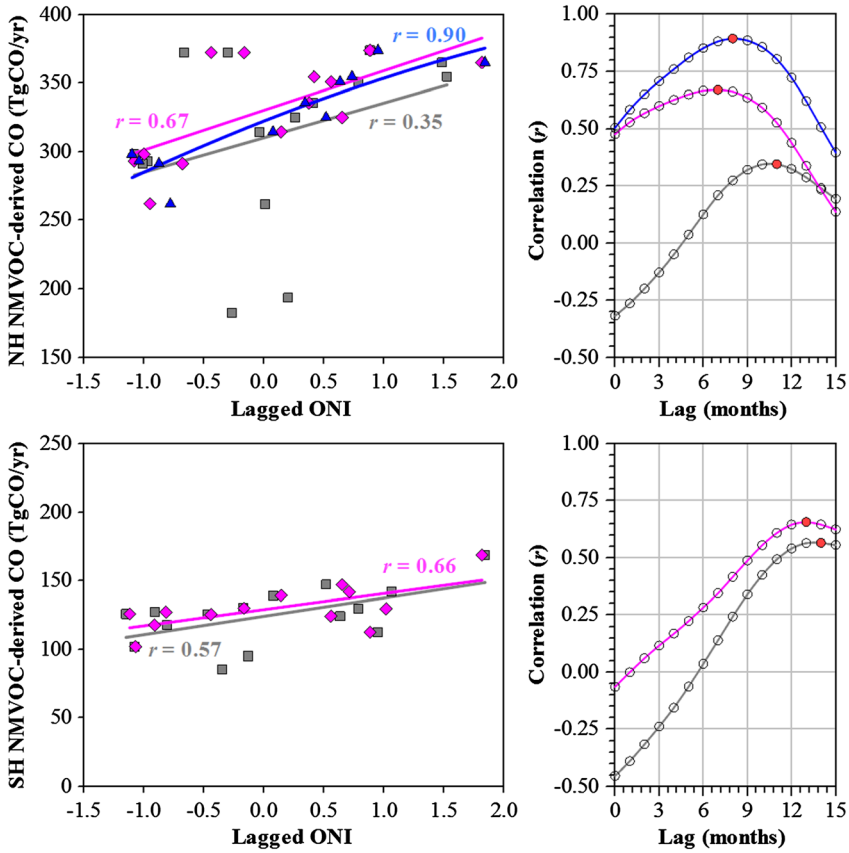

Figure 2. Correlation between lagged ONI and NMVOC-derived CO in each hemisphere (left panes) and the results of lag-correlation analysis (right panes). Lagged ONIs are acquired from the months showing the best correlation in the lag-correlation analyses (red dots). Correlation coefficients are calculated using all data points (grey), excluding 1/97 to 12/97 and 7/97 to 6/98 data (red), and excluding 1/97 to 12/97, 7/97 to 6/98, 1/01 to 12/01 and 7/01 to 6/02 data (blue).

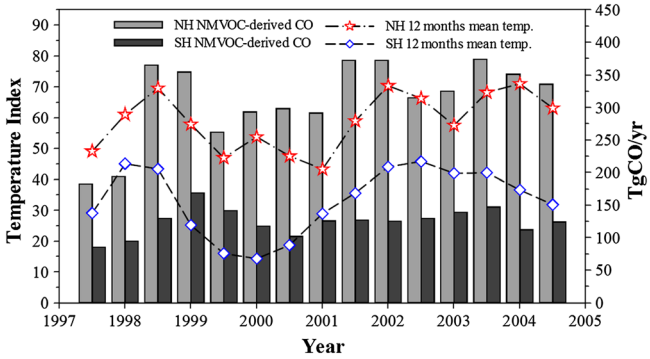

Figure 3. Time series showing the correlation between temperature and the hemispheric total NMVOC-derived CO. The light gray bars are the NH and the dark gray bars are the SH 1 year NMVOC-derived CO inventories. The stars and diamonds are the NH and the SH 1 year mean NASA GISS surface temperature index, respectively. The correlation (r) between temperature and NMVOC-derived CO was 0.58 in the NH and 0.01 in the SH.

offset is considered to be the sum of the intervals between ONI change and the change of actual terrestrial climate factors and the delayed response of plants from the changed climate conditions. Since the lifetime of CO is relatively long (average lifetime of 3 months), its variation is also smoothed and protracted from the NMVOC emission change. The shorter response time of the NH implies that there is a difference in NMVOC-derived CO production between the NH and SH in the extra-tropical regions where clear differences in vegetation distributions exist. Also, because the peak ONI month is usually in January and the maximum VOC emission is observed in summer of each hemisphere, the NH NMVOC-derived CO production responds faster than the SH. The slopes in the NH are steeper than SH since, in the NH, relatively more VOCs are emitted from the extra-tropical region where they are more sensitive to changes in the climate conditions. Also, in Figure 2, both the NH and SH showed robust positive correlations, with a stronger correlation in the SH. However, excluding the 1997–1998 low- and the 2001–2002 high-NMVOC-derived CO periods, the NH correlation between the lagged ONI and NMVOC-derived CO was strong ($r = 0.9$) as well (blue lines in Figure 2).

[15] Although normal or weak ENSO conditions were observed in 1996–1997 and 2001–2002, in the NH the former showed minimum NMVOC-derived CO through the whole inversion period and the latter unexpectedly increased 30% from the previous year. We investigate the correlation of NMVOC-derived CO and global temperature since biogenic NMVOC emissions are directly linked with temperature change [*Guenther et al.*, 1995]. In Figure 3, we illustrate the relation between CO production from NMVOC oxidation and global temperature change and the NASA Goddard Institute for Space Studies (GISS) land-ocean surface temperature index (http://data.giss.nasa.gov/gistemp/) [*Hansen et al.*, 1996; *Hansen et al.*, 2006; *Hansen et al.*, 2010].

[16] In the NH, the correlation between NMVOC-derived CO and temperature index ($r = 0.57$) is stronger than that with ONI ($r = 0.35$), indicating NMVOC-derived CO production is more correlated with temperature change in general. In contrast, in the SH, NMVOC-derived CO is weakly correlated with temperature ($r = 0.01$). This implies, in the SH, the chemical production of CO from NMVOC is influenced by a combination of factors rather than just temperature.

[17] The correlation between NMVOC-derived CO and tropical/extra-tropical temperature is also investigated (Figure 4). The NH NMVOC-derived CO is more strongly correlated with the extra-tropical temperature ($r = 0.9$) than the tropical temperature ($r = 0.3$), as well as having a steeper slope with extra-tropical temperature change. *Guenther et al.* [1995] shows that in the NH 65% of the NMVOCs are produced between the equator and 25°N and in the SH 90% of the emissions occur between the equator and 25°S. Thus, these highlight the significance of the NH extra-tropical region to the IAV of NMVOC-derived CO inventory in which NMVOC-derived CO production is primarily affected by temperature change. In the SH, neither tropical nor extra-tropical temperature distinctly impacts NMVOC-derived CO while the extra-tropical temperature showed slightly more robust correlation with temperature.

4. Summary and Conclusions

[18] In conjunction with NOAA GMD CO measurements and model simulations, a large average interannual variability of NMVOC-derived CO of 17.5% is observed during 1997–2004. We find that the IAV is correlated with the ENSO and surface temperature change. The impact of ENSO-induced climate conditions to NMVOC-derived CO

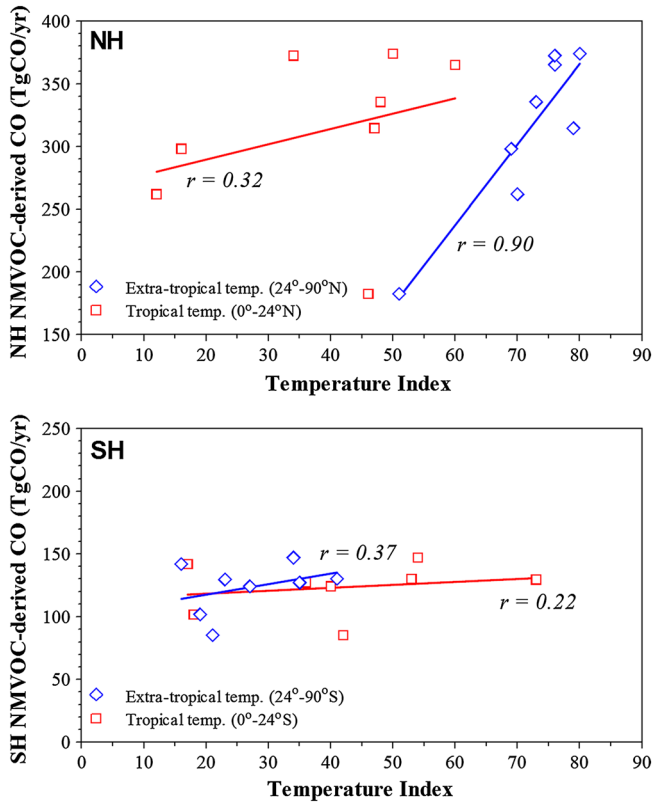

Figure 4. Correlation plots of *a posteriori* NMVOC-derived CO (NH: top, SH: bottom) versus tropical (red) and extra-tropical (blue) temperature index.

change is positively correlated. Furthermore, since the ONI changes about a year earlier than model simulated NMVOC-derived CO, ONI may be used as an indicator of future CO change. Global surface temperature is another important factor controlling NMVOC-derived CO production and shows a strong positive correlation with NH NMVOC-derived CO. A very strong correlation ($r = 0.9$) and steep slope was found between NMVOC-derived CO and extra-tropical temperature. Southern Hemisphere NMVOC-derived CO is weakly correlated with temperature. These observations lead us to surmise that, in the SH, ENSO (and not temperature) plays a primary role in the variation of NMVOC-derived CO. However, in the NH, both temperature and ENSO conditions need to be considered to explain the IAV of NMVOC-derived CO. Furthermore, since the IAV of the optimized NMVOC-derived CO production is significantly larger than previous modeling studies of isoprene emissions, this suggests that the global budgets of biogenic NMVOCs, or of their oxidation processes yielding CO, have greater variability than previously shown.

[19] **Acknowledgments.** We acknowledge the NOAA Earth System Research Laboratory Global Monitoring Division for surface CO, the NOAA/National Weather Service National Centers for Environmental Prediction Climate Prediction Center for Oceanic Niño Index and the NASA Goddard Institute for Space Studies for surface temperature. This work was supported by NSF grant ATM-0303727 and also partially supported by Korea Polar Research Institute grant (PE12410/ PG12030). The National Center for Atmospheric Research is funded by the National Science Foundation.

References

Arellano, A. F., Jr., P. S. Kasibhatla, L. Giglio, G. R. van der Werf, and J. T. Randerson (2004), Top-down estimates of global CO sources using MOPITT measurements, *Geophys. Res. Lett.*, *31*(1), L01104, doi:10.1029/2003GL018609.

Arellano, A. F., Jr., et al. (2006), Time-dependent inversion estimates of global biomass-burning CO emissions using Measurement of Pollution in the Troposphere (MOPITT) measurements, *J. Geophys. Res.*, *111*(D9), D09303, doi:10.1029/2005JD006613.

Bergamaschi, P., R. Hein, M. Heimann, and P. J. Crutzen (2000), Inverse modeling of the global CO cycle 1. Inversion of CO mixing ratios, *J. Geophys. Res.*, *105*(D2), 1909-1927, doi:10.1029/1999JD900818.

Duncan, B. N., et al. (2007), Global budget of CO, 1988-997: Source estimates and validation with a global model, *J. Geophys. Res.*, *112*(D22), D22301, doi:10.1029/2007JD008459.

Emmons, L. K., et al. (2010), Description and evaluation of the Model for Ozone and Related chemical Tracers, version 4 (MOZART-4), *Geosci. Model Dev.*, *3*, 43-67, doi:10.5194/gmd-3-43-2010.

Fowler, D., et al. (2009), Atmospheric composition change: Ecosystems-Atmosphere interactions, *Atmos. Environ.*, *43*(33), 5193-5267.

GLOBALVIEW-CO (2009), Cooperative Atmospheric Data Integration Project - Carbon Monoxide. CD-ROM, NOAA ESRL, Boulder, Colorado [Also available on Internet via anonymous FTP to ftp.cmdl.noaa.gov, Path: ccg/co/GLOBALVIEW].

Goldstein, A. H., and I. E. Galbally (2007), Known and Unexplored Organic Constituents in the Earth's Atmosphere, *Environ. Sci. Tech.*, *41*(5), 1514-1521, doi:10.1021/es072476p.

Granier, C., G. Pétron, J.-F. Müller, and G. Brasseur (2000), The impact of natural and anthropogenic hydrocarbons on the tropospheric budget of carbon monoxide, *Atmos. Environ.*, *34*(29-30), 5255-5270.

Guenther, A., et al. (1995), A global model of natural volatile organic compound emissions, *J. Geophys. Res.*, *100*(D5), 8873-8892, doi:10.1029/94JD02950.

Guenther, A., et al. (2006), Estimates of global terrestrial isoprene emissions using MEGAN (Model of Emissions of Gases and Aerosols from Nature), *Atmos. Chem. Phys.*, *6*(11), 3181-3210, doi:10.5194/acp-6-3181-2006.

Haddad, Z., et al. (2004), Global variability of precipitation to the Tropical Rainfall Measuring Mission, *J. Geophys. Res.*, *109*, D17103, doi:10.1029/2004JD004607.

Hansen, J., R. Ruedy, M. Sato, and R. Reynolds (1996), Global surface air temperature in 1995: Return to pre-Pinatubo level, *Geophys. Res. Lett.*, *23*(13), 1665-1668, doi:10.1029/96GL01040.

Hansen, J., et al. (2006), Global temperature change, *Proc. Natl. Acad. Sci. USA*, *103*(39), 14288-14293, doi:10.1073/pnas.0606291103.

Hansen, J., R. Ruedy, M. Sato, and K. Lo (2010), Global surface temperature change, *Rev. Geophys.*, *48*(4), RG4004, doi:10.1029/2010RG000345.

Heald, C. L., et al. (2004), Comparative inverse analysis of satellite (MOPITT) and aircraft (TRACE-P) observations to estimate Asian sources of carbon monoxide, *J. Geophys. Res.*, *109*(D23), D23306, doi:10.1029/2004JD005185

Horowitz, L. W., et al. (2003), A global simulation of tropospheric ozone and related tracers: Description and evaluation of MOZART, version 2, *J. Geophys. Res.*, *108*(D24), 4784, doi:10.1029/2002JD002853.

Kalnay, E., et al. (1996), The NCEP/NCAR 40-Year Reanalysis Project, *B. Am. Meteorol. Soc.*, *77*(3), 437-471, doi:10.1175/1520-0477(1996)077<0437:TNYRP>2.0.CO;2.

Kasibhatla, P., A. Arellano, J. A. Logan, P. I. Palmer, and P. Novelli (2002), Top-down estimate of a large source of atmospheric carbon monoxide associated with fuel combustion in Asia, *Geophys. Res. Lett.*, *29*(19), 1900, doi:10.1029/2002GL015581.

Kistler, R., et al. (2001), The NCEP–NCAR 50–Year Reanalysis: Monthly Means CD–ROM and Documentation, *B. Am. Meteorol. Soc.*, *82*(2), 247-267, doi:10.1175/1520-0477(2001)082<247:TNNYRM>2.3.CO;2.

Lathière, J., et al. (2006), Impact of climate variability and land use changes on global biogenic volatile organic compound emissions, *Atmos. Chem. Phys.*, *6*(8), 2129-2146, doi:10.5194/acp-6-2129-2006.

Lawrence, M. G., P. Jöckel, and R. von Kuhlmann (2001), What does the global mean OH concentration tell us?, *Atmos. Chem. Phys.*, *1*(1), 37–49, doi:10.5194/acp-1-37-2001.

Mak, J. E., and C. A. M. Brenninkmeijer (1998), Measurement of ^{13}CO and $C^{18}O$ in the free troposphere, *J. Geophys. Res.*, *103*(D15), 19,347–19,358, doi:10.1029/97JD02502.

Miyoshi, A., S. Hatakeyama, and N. Washida (1994), OH radical- initiated photooxidation of isoprene: An estimate of global CO production, *J. Geophys. Res.*, *99*(D9), 18,779–18,787, doi:10.1029/94JD01334.

Müller, J. F., and T. Stavrakou (2005), Inversion of CO and NOx emissions using the adjoint of the IMAGES model, *Atmos. Chem. Phys.*, *5*(5), 1157-1186, doi:10.5194/acp-5-1157-2005.

Müller, J. F., et al. (2008), Global isoprene emissions estimated using MEGAN, ECMWF analyses and a detailed canopy environment model, *Atmos. Chem. Phys.*, *8*(5), 1329-1341, doi:10.5194/acp-8-1329-2008.

Naik, V., C. Delire, and D. J. Wuebbles (2004), Sensitivity of global biogenic isoprenoid emissions to climate variability and atmospheric CO_2, *J. Geophys. Res.*, *109*(D6), D06301, doi:10.1029/2003JD004236.

Novelli, P. C., K. A. Masarie, and P. M. Lang (1998), Distributions and recent changes of carbon monoxide in the lower troposphere, *J. Geophys. Res.*, *103*(D15), 19,015–19,033, doi:10.1029/98JD01366.

Ohara, T., et al. (2007), An Asian emission inventory of anthropogenic emission sources for the period 1980-2020, *Atmos. Chem. Phys.*, *7*, 4419-4444, doi:10.5194/acp-7-4419-2007.

Olivier, J., and J. Berdowski (2001), Global emissions sources and sinks, in The Climate System, edited by J. Berdowski, R. Guicherit and B. J. Heij, pp. 33-78, Balkema Publishers/Swets & Zeitlinger Publishers, Lisse, The Netherlands.

Olivier, J., et al. (2003), Present and future surface emissions of atmospheric compounds, *POET repo*rt #2, EU project EVK2-1999-00011.

Palmer, P. I., et al. (2003), Inverting for emissions of carbon monoxide from Asia using aircraft observations over the western Pacific, *J. Geophys. Res.*, *108*(D21), 8828, doi:10.1029/2003JD003397.

Palmer, P. I., et al. (2006), Using CO_2:CO correlations to improve inverse analyses of carbon fluxes, *J. Geophys. Res.*, *111*(D12), D12318, doi:10.1029/2005JD006697.

Park, K. (2010), Joint Application of Concentration and Isotope Ratios to Investigate the Global Atmospheric Carbon Monoxide Budget: An Inverse Modeling Approach, Ph.D. Thesis, Stony Brook University, Stony Brook, NY, USA.

Pétron, G., et al. (2002), Inverse modeling of carbon monoxide surface emissions using Climate Monitoring and Diagnostics Laboratory network observations, *J. Geophys. Res.*, *107*(D24), 4761, doi:10.1029/2001GD001305.

Pétron, G., et al. (2004), Monthly CO surface sources inventory based on the 2000-2001 MOPITT satellite data, *Geophys. Res. Lett.*, *31*(21), doi:L2110710.1029/2004GL020560.

Pfister, G. G., et al. (2008), Contribution of isoprene to chemical budgets: A model tracer study with the NCAR CTM MOZART-4, *J. Geophys. Res.*, *113*(D5), D05308, doi:10.1029/2007JD008948.

Shindell, D. T., et al. (2007), Climate response to projected changes in short-lived species under an A1B scenarioi from 2000-2050 in the GISS climate model, *J. Geophys. Res.*, *112*, D20103, doi:10.1029/2007JD008753.

Shindell, D. T., et al. (2008), Multimodel projections of climate change from short-lived emissions due to human activities, *J. Geophys. Res.*, *113*, D11109, doi:10.1029/2007JD009152.

Smith, T. M., R. W. Reynolds, T. C. Peterson, and J. Lawrimore (2008), Improvements to NOAA's Historical Merged Land–Ocean Surface Temperature Analysis (1880–2006), *J. Climate*, *21*(10), 2283-2296, doi:10.1175/2007JCLI2100.1.

Staudt, A. C., et al. (2001), Continental sources, transoceanic transport, and interhemispheric exchange of carbon monoxide over the Pacific, *J. Geophys. Res.*, *106*(D23), 32571-32589, doi:10.1029/2001JD900078.

Tie, X., A. Guenther, and E. Holland (2003), Biogenic methanol and its impacts on tropospheric oxidants, *Geophys. Res. Lett.*, *30*(17), 1881, doi:10.1029/2003GL017167.

van der Werf, G. R., et al. (2006), Interannual variability in global biomass burning emissions from 1997 to 2004, *Atmos. Chem. Phys.*, *6*, 3423–3441, doi:10.5194/acp-6-3423-2006.

Wang, Y., J. A. Logan, and D. J. Jacob (1998), Global simulation of tropospheric O_3-NOx -hydrocarbon chemistry 2. Model evaluation and global ozone budget, *J. Geophys. Res.*, *103*(D9), 10727-10755, doi:10.1029/98JD00157.

Williams, J., et al. (2002), Near equatorial CO and O_3 profiles over the Indian Ocean during the winter monsoon: High O_3 levels in the middle troposphere and interhemispheric exchange, *J. Geophys. Res.*, *107*(D19), 8007, doi:10.1029/2001JD001126.